

Full Length Article

Particle size dependence of nanoclustered ceria abrasives on surface activity and chemical mechanical planarization performance



Na-Yeon Kim ^{a,b,1}, Uiseok Hwang ^{c,1}, Jaeuk Sung ^{d,e}, In-Kyung Park ^c, Taesung Kim ^f, Jonghwan Suhr ^{c,f}, Jae-Do Nam ^{a,b,c,*}

^a Department of Energy Science, Sungkyunkwan University, Suwon 16419, Republic of Korea

^b Bead Origin Inc., Suwon 16419, Republic of Korea

^c Department of Polymer Science and Engineering, Sungkyunkwan University, Suwon 16419, Republic of Korea

^d Department of Applied Data Science, Sungkyunkwan University, Suwon 16419, Republic of Korea

^e Samsung Electronics Co., Ltd., Suwon 16677, Republic of Korea

^f School of Mechanical Engineering, Sungkyunkwan University, Suwon 16419, Republic of Korea

ARTICLE INFO

Keywords:

Chemical mechanical planarization

Cerium oxide

Crystallinity

Surface activity

Removal rate

Semiconductors

ABSTRACT

The particle size of cerium oxide (ceria) abrasives plays a crucial role in the design and development of advanced self-stopping slurries for the chemical mechanical planarization (CMP) process in semiconductor device manufacturing. However, a lack of ceria nanoparticles (NPs) with a narrow size distribution and uniform shape poses challenges in investigating the fundamental principles of the relationship between abrasive size and CMP performance. In this study, we thoroughly investigated the effect of ceria NP size on the removal rate (RR) of silicon oxide using uniform-sized nanoclustered (NC) ceria NPs with three diameters: 51.4 nm (NC51), 68.6 nm (NC69), and 108.0 nm (NC108). While all three types of ceria NPs shared a crystallinity of ~ 70.6 %, they exhibited distinct physicochemical characteristics. As the particle size decreased, the specific surface area and chemical activity (i.e., $\text{Ce}^{3+}/\text{Ce}^{4+}$) increased by 155 % and 69 %, respectively. In the CMP process, where direct contact between the abrasives and wafer occurs, the abrasive size influences CMP performance. Experimentally, NC51 achieved the highest RR among the three slurries, along with complex size-dependent contact properties and chemical activities. These experimental results offer significant insights into precise semiconductor manufacturing in a practical manner.

1. Introduction

As electronic devices and their semiconductor components continue to become more compact, cutting-edge technology must be adopted to meet the increasing complex requirements of semiconductor devices and to enhance their performance [1]. For example, according to the semiconductor roadmap, the wiring width of semiconductors has decreased to 3 nm or less since 2015. Simultaneously, the number of semiconductor layers has increased, reaching 321 layers in 2023 (SK Hynix Co., Ltd., Korea). With the emergence of ultraprecision semiconductor processing technology, which can achieve wiring widths of less than 10 nm and arrangements of more than 100 semiconductor layers, these wafer manufacturing processes now necessitate an extremely high level of repeatability and uniformity to enable enhanced device yields and

cost reduction [2]. Therefore, the abrasives and slurries used in the chemical mechanical planarization (CMP) process are crucial for reducing scratches or defects, which are directly related to chip yields and manufacturing costs.

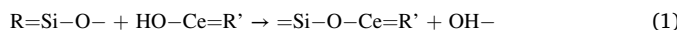
The CMP process is critical for nanolevel planarization, smoothing out uneven and rough surfaces caused by insulating films or metal layers deposited on a wafer. The CMP process has three main applications: the formation of transistors (front-end-of-line, FEOL), local connections between transistors (middle-of-line, MOL), and interconnected structures (back-end-of-line, BEOL). Among these, in the FEOL process of constructing the device architecture, a crucial step is polishing the SiO_2 (silicon oxide; silica) substrate to planarize it and creating precise dielectric sites to accurately separate two adjacent active device regions. Because the CMP slurries used in the FEOL process require auto-stopping

* Corresponding author.

E-mail address: jdnam@skku.edu (J.-D. Nam).

¹ Na-Yeon Kim and Uiseok Hwang contributed equally to this work.

or self-stopping capabilities, CeO₂ (cerium oxide; ceria) nanoparticles (NPs) are primarily used as abrasives as they afford excellent removal rates (RRs) via chemical reactions with the silica insulator and owing to their self-stopping properties on the SiO₂ substrate [3]. The polishing mechanism between the ceria abrasives and SiO₂ substrate is as follows [4,5]:



In this process, a strong bond is formed between Ce and the hydrated silicate, and subsequently, the Si-O-Ce lump is removed from the wafer surface. Note that requirements that are more stringent are necessary for ceria abrasives, particularly as semiconductor devices become increasingly miniaturized, thereby necessitating higher chip product yields. Therefore, the semiconductor industry requires colloidal or wet-type ceria abrasives with adjustable sizes and narrow size distributions.

Successful CMP depends on several factors, including the desired material RR, selectivity, planarity degree – within wafer non-uniformity (WIWNU) and within die non-uniformity (WIDNU), defectivity, and surface quality. Among these factors, a high RR and self-stopping properties are the most fundamental in SiO₂-polishing, and they are known to be related to the electronic hybridization properties of ceria abrasives, as they are associated with the formation of Si-O-Ce chemical bonds [6]. The trivalent state of the cerium atom, Ce³⁺, is considered a chemically active site on the ceria surface and is one of the key factors influencing chemical reactions in the CMP process [6–10]. The ratio of Ce³⁺/Ce⁴⁺, commonly regarded as surface activity, has been experimentally determined to be influenced by the shape and crystallinity of the abrasive particles. For example, the ratio of Ce³⁺/Ce⁴⁺ in ceria NPs increases with decreasing crystallinity. We have also previously reported that nanoclustered (NC) ceria abrasives consisting of ~ 5 nm NPs can contain a high proportion of Ce³⁺ and thus outperform cubic-fluorite ceria abrasives with high crystallinity.

However, to the best of our knowledge, an experimental demonstration of the effect of particle size on the Ce³⁺/Ce⁴⁺ ratio and overall CMP performance is still lacking. Ceria NPs with a narrow size distribution and consistent shapes are difficult to obtain owing to the challenges associated with their preparation. Consequently, the relationship between abrasive size and surface activities of ceria during CMP processing has not been clearly identified. Given that the polishing process involves the direct contact of abrasive particles with the wafer surface, a higher CMP performance is attributed to the optimization of the contact properties between the abrasives and wafer substrate. Therefore, in addition to the chemical properties of the abrasives, their size-dependent characteristics, such as the number of contacts, contact area, and momentum (or impulse) to the wafer, can influence polishing performance metrics such as RR, scratch formation, dishing, erosion, WIWNU, and WIDNU. Thus, the relationship between the size dependence of abrasive particles and SiO₂ polishing performance in the development of wet ceria-based slurries for highly advanced semiconductor chip manufacturing must be understood.

In this study, the surface and crystal characteristics and the polishing properties of NC-ceria particles with three sizes were compared. The size dependence of the abrasive particles on the polishing properties could be accurately identified because the size distribution of the ceria NPs was narrow, and they were spherical. All three NC-ceria samples exhibited a low crystallinity of ~ 70 %. As their average size decreased, both the Brunauer–Emmett–Teller (BET) surface area and number of chemically active sites (Ce³⁺) on the NC-ceria samples increased. However, the SiO₂ RR did not improve as much as the increase in the chemical activity (Ce³⁺/Ce⁴⁺) and surface area of the ceria NPs with their size reduction. This is because, when the abrasives in the slurry collided with the wafer, they were subjected to different impact effects, such as the number of contacts (N_p), contact area (S_p), and momentum (M_p), depending on the particle diameter. Overall, NC-ceria exhibited RR characteristics superior to those of conventional commercial cubic fluorite ceria abrasive

particles, and they may be effective in reducing scratch defects. Our experimental demonstrations contribute to a collective understanding of the size dependence of abrasives, which can be used to effectively design CMP slurries and to predict polishing performance by integrating the wafer contact and surface chemical characteristics of ceria.

2. Experimental section

2.1. Materials

The three dispersions of commercially available colloidal ceria NPs in deionized water (BOC S40, S70, and M10) were obtained from Bead Origin, Inc. (Korea) [6,11,12]. These ceria NPs were named based on their structural characteristics and average size. For example, all three groups of particles had a nanoclustered structure (NC-ceria), which were synthesized in the liquid phase; detailed information can be found in references [6,12]. The primary sizes of the NC-ceria NPs, as measured via transmission electron microscopy (TEM), were 51.4 nm (NC51), 68.6 nm (NC69), and 108.0 nm (NC108) for S40, S70, and M10, respectively (see Fig. 1). Additionally, the commercial colloidal ceria dispersion of Zenus® HC60 (Solvay, Ltd., Belgium) [13,14] was used as a reference for comparison; these ceria NPs were named CF-ceria based on their cubic fluorite-structured appearance. Other commercial ceria NPs were obtained from Cabot Electronics Co. (USA) (D7400) and Sigma-Aldrich (USA).

2.2. Characterization of the ceria NPs

The morphology and structure of the ceria NPs were characterized via field-emission scanning electron microscopy (FESEM) (JEOL JSM 7401F, Japan) and high-resolution TEM (HRTEM) (JEM-2100F, Japan). X-ray diffraction (XRD) patterns were obtained using an X-ray diffractometer (Rigaku Smart Lab SE, Japan) with Cu K α radiation ($\lambda = 0.15406$ nm) at a scanning speed of 0.02°/s. BET surface area measurements were conducted using a Micromeritics TriStar II 3020 (USA) via nitrogen adsorption–desorption isotherms. The elemental composition was determined using X-ray photoelectron spectroscopy (XPS) (ESCALAB 250, Thermo, USA). The zeta potential and hydrodynamic radius of the NPs were measured using laser Doppler electrophoresis and dynamic light scattering (DLS), respectively (Zetasizer Nano-ZS, Malvern, UK).

2.3. Preparation of CMP slurries

CMP slurries were prepared by dispersing the ceria NPs as abrasives in deionized water at a concentration of 0.3 wt% without any additives. Although the pH values of all slurries were not adjusted such that only the properties of the pure abrasives could be compared, the pH values of all slurries ranged from 4 to 4.6, which falls within the manufacturing conditions of CMP in practice.

2.4. CMP performance evaluation

CMP was performed using a CMP polisher (GNP POLI-400L, G&P Technology Inc., Korea) for 1 min at a fixed head pressure of 4 psi. The flow rate of the slurry was 150 mL/min and the rotation speed of the polishing pad/wafer was 93/87 rpm during the CMP process. The SiO₂ wafer used in the process was a 40 × 40 mm² coupon wafer (SiO₂ thickness of the bare wafer = 30,000 Å). A polyurethane polishing pad (HD-319C, SKC Inc., Korea) and conditioner (CI-45, Saesol Diamond Co., Ltd., Korea) were used for the CMP process. Pad conditioning was conducted for 5 min between changes in the slurry. The RR was evaluated by measuring the thickness of the SiO₂ at five points 5 mm apart using a reflectometer (ST4000-DLX, Korea) before and after the polishing process.

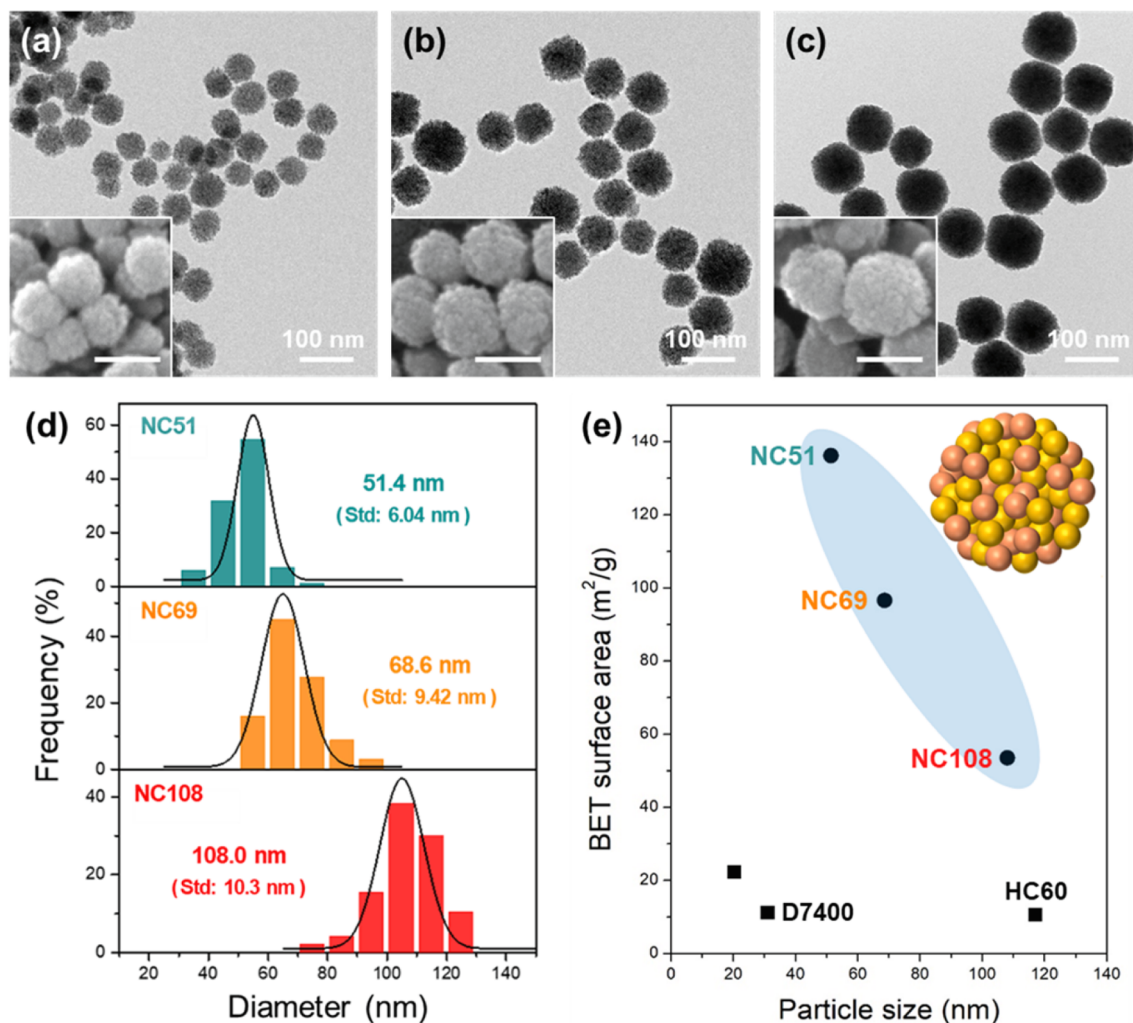


Fig. 1. TEM images of (a) NC51, (b) NC69, and (c) NC108 with insets showing the corresponding SEM images for each NP. (d) Size distribution histograms of NC51, NC69, and NC108. (e) BET surface areas of NC51, NC69, and NC108, compared with those of other commercially available ceria NPs.

3. Results and discussion

3.1. Morphology of NC-ceria NPs

Fig. 1a–c show the TEM and SEM images of the three types of NC-ceria NPs: NC51, NC69, and NC108, illustrating their shape and size. All three ceria NPs exhibit a round surface morphology and are highly monodisperse in size. NC51, NC69, and NC108 have average diameters of 51.5, 68.6, and 108.0 nm with low standard deviations of 6.04, 9.42, and 10.3 nm, respectively (Fig. 1d), indicating extremely narrow size distributions. Overall, NC-ceria abrasives are likely advantageous in reducing scratches or dishing defects in the CMP process owing to their smooth surface and round shapes, in contrast to the pointed angles or sharp edges commonly found in CF-ceria abrasives (Fig. S1 and S2 in the Supporting Information). Specifically, highly crystallized ceria abrasives, like Zenus® HC60, have been widely employed in the CMP process of the semiconductor industry due to their narrower size distribution compared to typical calcined ceria particles [14]. However, they exhibit sharp edges originating from their large crystallites (Fig. S1), which could potentially lead to microscopic scratches. Moreover, advanced semiconductors requiring exceptionally high resolution may demand a novel colloidal ceria abrasive type to attain “zero” scratches and optimize chip yield while retaining a high RR, a feat potentially attainable with extremely monodisperse spherical abrasives [6,31,32].

The rough surface of the NC-ceria NPs, covered with small dots (as

observed in the SEM images in the insets of Fig. 1a–c), is a unique feature that was extensively discussed in our previous study [6]. These characteristics originate from the nanoclustered structure of NC-ceria, which consists of fine granules measuring 4–6 nm in size, thus providing a considerably larger surface area compared to that provided by calcined or crystalline ceria particles. As shown in Fig. 1e and Table S1, the BET surface area of ceria NPs substantially increases with a decrease in particle size. The overall BET surface area increases by more than two times, from 53.5 to 136.2 m²/g, which is unusual, given that the particle size has almost halved from 108.0 to 51.4 nm. These values surpass those of other commercially available ceria NPs, such as 10.6 m²/g for Zenus® HC60 and 11.2 m²/g for D7400.

3.2. Crystal characteristics of NC-ceria NPs

The crystal characteristics of NC51, NC60, and NC108 were evaluated using their XRD patterns, as shown in Fig. 2a. The NPs exhibit characteristic peaks of the cubic-fluorite lattice of the Ce and O atoms of ceria at 28.55°, 33.08°, 47.47°, 56.33°, 59.08°, 69.4°, 76.7°, and 79.07°, corresponding to the (1 1 1), (2 0 0), (2 2 0), (3 1 1), (2 2 2), (4 0 0), (3 3 1), and (4 2 0) lattice planes, respectively, according to card No. 34–0394 of the Joint Committee on Powder Diffraction Standards (JCPDS). These NC-ceria NPs exhibited relatively broad XRD patterns with full width at half maximum (FWHM) values of 1.52°, 1.40°, and 1.88° for the (1 1 1) peaks, demonstrating that the NPs possessed small crystallites and a low

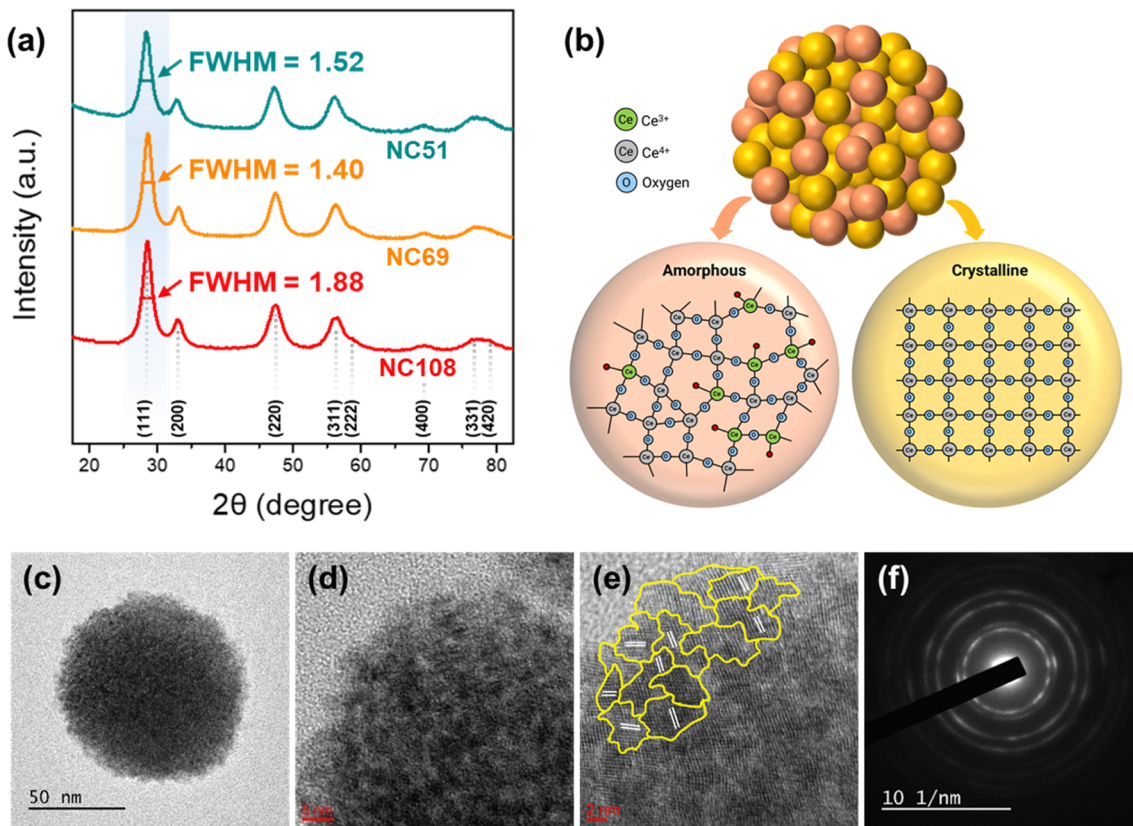


Fig. 2. (a) XRD patterns of NC51, NC69, and NC108. (b) Schematic illustration of the NC-ceria NPs composed of amorphous and crystalline ceria domains, along with the atomic arrangement of Ce and O. (c–e) TEM images of NC51 and (f) the corresponding SAED pattern.

degree of crystallinity. The average crystallite size (L_c) of the ceria NPs was quantitatively calculated using the Scherrer equation and the FWHM value, as follows:

$$L_c = \frac{K \cdot \lambda}{\beta \cdot \cos\theta} \quad (2)$$

where λ is the X-ray wavelength (nm), β is the FWHM in radians, and K is a constant related to crystal shape, considered 0.9 in this study [15]. The crystallinity (X_c) of the ceria NPs was evaluated by determining the area under the XRD peaks using the Ruland-Vonk method [16], as follows:

$$X_c (\%) = \frac{I_c}{I_c + I_a} \times 100 \quad (3)$$

where I_c is the sum of the areas under the crystalline peaks and I_a is the area of the amorphous halo. Table S1 summarizes the quantitatively calculated crystallite size (L_c) and crystallinity (X_c) values of the NC-ceria NPs. The crystallite sizes are 5.40, 5.86, and 4.36 nm for NC51, NC69, and NC108, respectively. Thus, the three NC-ceria NPs are composed of fine crystallites with an average size of $L_c = 5.21$ nm and a crystallinity of $X_c = 70.6\%$. In stark contrast, the crystallite size of the CF-ceria (i.e., Zenus® HC60), $L_c = 45.5$ nm, is almost half of the particle size (117.0 nm), suggesting that the entire particle is grown as one or two single crystals; this inference is supported by $X_c = 95.8\%$. The average 5.21 nm-sized crystallites of NC-ceria NPs, which can be either crystalline or amorphous, agglomerate and form the nanoclustered structure of ceria particles, as schematically shown in Fig. 2b. These crystal characteristics are directly confirmed in the TEM images and selected area electron diffraction (SAED) patterns shown in Fig. 2c–f. We could delineate phase boundaries, as shown in Fig. 2e, using the lattice planes that appeared to be oriented in different directions. Each yellow-bordered crystallite is either the crystalline phase, which is characterized by white parallel lines with a 3.10 Å d-spacing and corresponds to

the (111) lattice plane of ceria, or the amorphous phase, where none of these lines are visible. The granule sizes observed in the TEM images ranged from 3–6 nm, corresponding to a crystallite size of $L_c = 5.21$ nm, as determined from the XRD analysis. The diffused SAED pattern in Fig. 2f further supports the idea that the NC-ceria NPs possessed crystallites in both crystalline and amorphous phases, as represented by clear spots and diffused rings, respectively.

Specifically, approximately 29.4 % of the single ceria NP was in the amorphous phase. Generally, the crystalline phase refers to a material with a highly regular atomic arrangement. In contrast, the irregular atomic arrangement of amorphous phases can result in numerous incompletely bound atoms (dangling bonds). A greater proportion of the amorphous phase in the particle can lead to a higher number of available active sites, which can participate in chemical reaction applications, such as catalysis, glass polishing, and semiconductor manufacturing. The chemically active site in ceria is typically Ce³⁺, which lacks an oxygen atom and possesses chemically unpaired electrons. NC-ceria may be more likely to accelerate the formation of chemical bonds with other materials, given that a significant portion (29.4 %) of the amorphous ceria is located on its surface. Particularly in the CMP process, NC-ceria abrasives can accelerate the formation of Ce–O–Si bonds between the ceria abrasive and SiO₂ substrate, thereby enhancing the RR properties.

3.3. Surface activity of NC-ceria NPs

XPS analysis was conducted on the NC-ceria NPs to obtain quantitative data regarding the chemically active sites (i.e., Ce³⁺) present on their surfaces, as shown in Fig. 3. The Ce 3d peaks are split into the Ce 3d_{5/2} and Ce 3d_{3/2} ionizations, which are labelled as v_0, v_1, v_2, v_3 , and v_4 for Ce 3d_{5/2}, and as u_0, u_1, u_2, u_3 , and u_4 for Ce 3d_{3/2}. Among these, the v_0, v_2, u_0 , and u_2 peaks represent the characteristics of Ce³⁺ ions, whereas the v_1, v_3, v_4, u_1, u_3 , and u_4 peaks represent those of the Ce⁴⁺

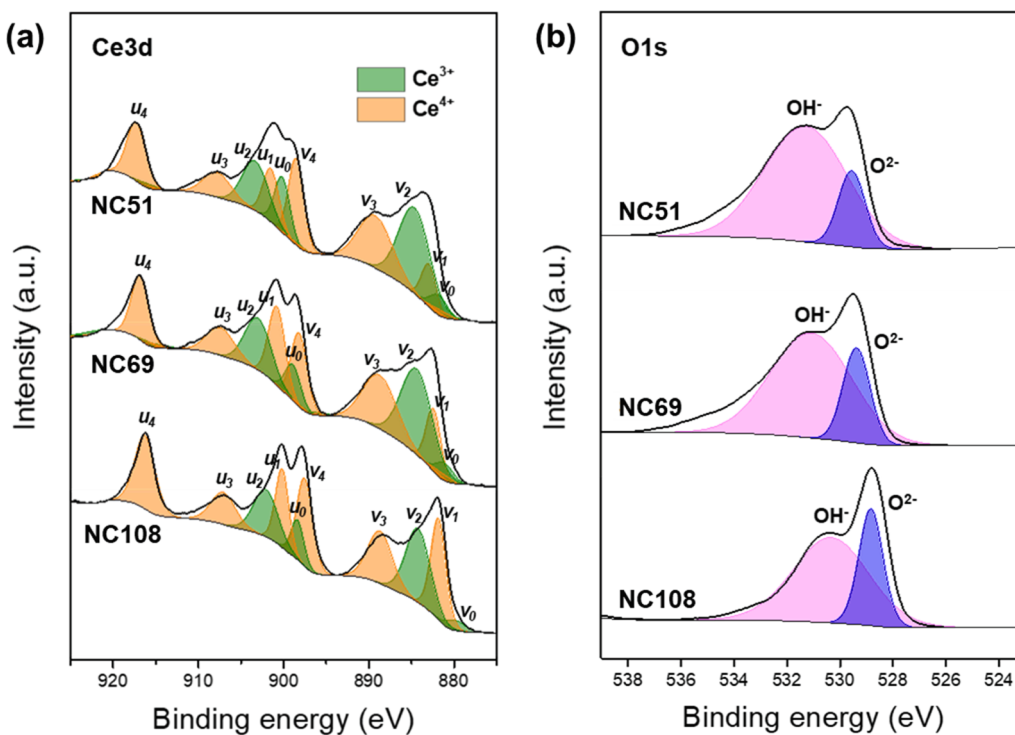


Fig. 3. XPS (a) Ce 3d and (b) O 1s core-level spectra of NC51, NC69, and NC108.

ions [17]. We calculated the concentrations of Ce³⁺ and Ce⁴⁺ using the following v and u assignments: $[Ce^{3+}] = v_0 + v_2 + u_0 + u_2$ and $[Ce^{4+}] = v_1 + v_3 + v_4 + u_1 + u_3 + u_4$. The calculated Ce³⁺ concentrations for NC51, NC69, and NC108 were 45.0 %, 41.0 %, and 32.6 %, respectively (detailed information on each XPS peak assignment is provided in Table S2). Specifically, each ceria NP contained Ce^{3+}/Ce⁴⁺ ratios of 81.7 %, 69.4 %, and 48.4 %. This result indicates that the number of chemically active sites of NC-ceria NPs increased with decreasing size, which is consistent with previous studies on size and surface activity, e.g., 17 % for 30-nm NPs and 44 % for 3-nm NPs [18–21].}

In an aqueous system, the Ce³⁺ ions on the ceria NP surfaces act as chemically active sites to promote the dissociation of water, resulting in the formation of hydroxyl groups (OH⁻) on the NP surface [22,23]. These hydroxyl groups on the NP surface subsequently function as active sites for the chemical and physical adsorption of other materials [24], resulting in the formation of Ce–O–Si bonds during the CMP process [4,25]. The concentrations of hydroxyl groups on the NC-ceria NPs can be determined via O 1 s XPS core-level spectra, as shown in Fig. 3b; Table S2 summarizes the details of the two peaks assigned to the lattice oxygen (O²⁻) and surface hydroxyl group (OH⁻) [26,27]. The proportions of hydroxyl groups for NC51, NC69, and NC108 were 82.4 %, 76.8 %, and 69.4 %, respectively, indicating that the number of hydroxyl groups on the NP surface generally increased with decreasing particle size. Notably, these concentrations are higher than those in CF-ceria (47.3 %). This result is consistent with the finding that NC-ceria has a significantly higher concentration of Ce³⁺ on its surface compared with CF-ceria, which can be understood using the schematic shown in Fig. 2b. Collectively, with a decrease in the size of the nanocluster agglomerates, the surface area of the NP increases rapidly, and simultaneously, the concentration of hydroxyl groups on the NP surface proportionally increases with that of Ce³⁺ [28]. Consequently, in the CMP process, the NC-ceria abrasives have a larger number of Ce–OH active sites on their surfaces compared with the CF-ceria abrasives, which subsequently are likely to accelerate the formation of Ce–O–Si bonds between the particles and SiO₂ substrate, thereby improving the CMP performance.

To provide further insight into the ceria NPs, we compared the

surface activity and crystallinity of various NC- and CF-ceria NPs, as shown in Fig. 4a and 4b, respectively. We demonstrated that the size of the NC-ceria NPs and the Ce³⁺/Ce⁴⁺ ratio were inversely proportional. In terms of absolute quantities, the NC-ceria NPs exhibited a considerably higher surface activity than that of the conventional CF-ceria NPs, regardless of the particle size (Fig. 4a). This result strongly suggests that the particle size, morphology, and crystal characteristics should be collectively considered to evaluate and predict the surface activity of various types of ceria NPs. Specifically, the crystallinity of the NC-ceria NPs was lower than that of typical CF-ceria NPs, as shown in Fig. 4b. The presence of fine granules consisting of single particles and oxygen vacancies at the grain boundaries contributed to the decrease in the crystallinity of the NC-ceria NPs while simultaneously enhancing the concentration of chemically active sites (i.e., Ce³⁺). Amorphous crystallites with irregular dangling bonds constituted 29.4 % of the NC-ceria NPs, resulting in a crystallinity of 70.6 %.

3.4. Key parameters of abrasive particles in the CMP process

The size dependence of the morphological, crystalline, and surface characteristics of the ceria NPs discussed herein may be related to the abrasive characteristics observed in the CMP slurries, such as the RR, scratch formation, dishing, erosion, WIWNU, and WIDNU. Variations in the size of abrasive particles in the slurry correspond to predictable fluctuations in CMP performance. For example, during the CMP process, abrasives disperse and rotate with water in the gap between the polishing pad and patterned wafer. In this process, the sizes of abrasive particles (R_p) theoretically influence several quantities that subsequently affect CMP performance: the number of wafer touches of abrasive particles (N_p), the wafer contact area of abrasive particles (S_p) (assuming a spherical shape), and the momentum (or impulse) of the abrasive particles (M_p) when they collide with the wafer surface. More specifically, N_p is proportional to the solid content (C) divided by the particle volume ($4/3 \pi R_p^3$), resulting in the following relation:

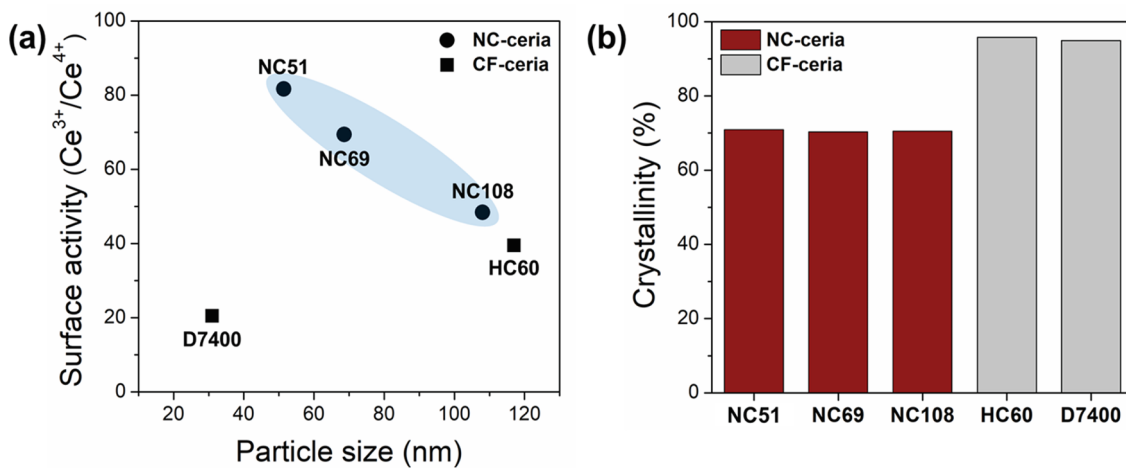


Fig. 4. (a) Surface activity ($\text{Ce}^{3+}/\text{Ce}^{4+}$) and (b) crystallinity of ceria for various NC- and CF-ceria NPs.

$$N_p \propto \frac{C}{R_p^3} \quad (4)$$

RR increases with N_p because a larger number of abrasive contacts provides more opportunities for the wafer to be abraded. Additionally, larger particles result in a lower RR if the solid content is identical.

The S_p of a sphere placed on a flat surface is proportional to the surface area of the sphere ($4\pi R_p^2$), as follows:

$$S_p \propto R_p^2 \quad (5)$$

Equation (5) suggests that the wafer contact area of the abrasive particles would be proportional to the RR, subsequently implying that larger particles would result in a higher RR in the CMP process, which is consistent with the findings from a previous study [29].

Another important quantitative parameter related to abrasive particle size is the momentum generated by the collision of particles with the wafer surface. This momentum (M_p) is proportional to the mass and velocity of the moving particles. Thus, the following relation can easily be derived, neglecting the drag force related to velocity:

$$M_p \propto R_p^3 \quad (6)$$

As observed in this relationship, larger particles exert a larger impact (or stress) on the wafer surface, resulting in a higher RR.

According to Eqs. (4)–(6), if the abrasive particle size is reduced, N_p increases, but S_p and M_p decrease, and vice versa. Conversely, as the particle size increases, the momentum becomes more substantial; however, the particle also becomes heavier. Thus, effective contact between the particle and the wafer substrate, which is positioned above the pad during the CMP process, cannot be confirmed. Thus, the CMP process involves a complex interplay of a particle system that includes not only all the physical quantities, namely N_p , S_p , and M_p , but also chemical functions such as the $\text{Ce}^{3+}/\text{Ce}^{4+}$ ratio.

3.5. Performances of ceria slurries in the CMP process

Fig. 5a illustrates the electrokinetic properties of the NC-ceria NPs, as evaluated via zeta potential measurements. At pH 4, which corresponds to the CMP operating conditions in actual semiconductor manufacturing processes, all ceria slurry samples exhibited high zeta potentials exceeding 30 mV, indicative of a stable dispersion state achieved via electrostatic repulsion [30]. Silica typically exhibits a negative surface charge, especially around pH 4. Therefore, in the CMP process under these pH conditions, ceria abrasives are likely to interact with the SiO_2 substrate via electrostatic attraction stemming from the opposite charges between them. Notably, the zeta potential value tended to increase slightly as the size of the NC-ceria NPs increased. This trend can be attributed to a higher concentration of hydroxyl groups on the surface, which decreases with particle size, as confirmed via XPS analysis.

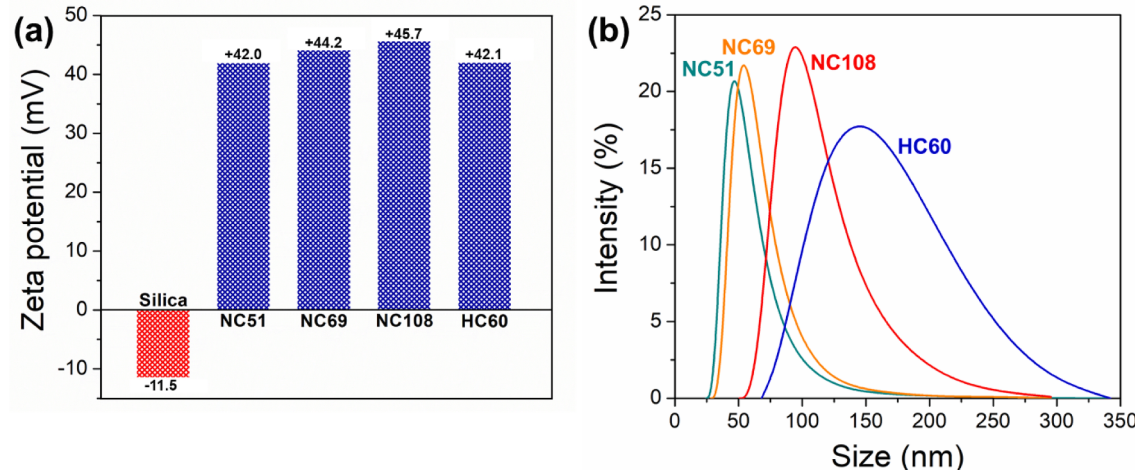


Fig. 5. (a) Zeta potential comparison between NC51, NC69, and NC108 ceria NPs and CF-ceria (HC60), as well as silica NPs in an aqueous system at pH 4 and (b) corresponding hydrodynamic radius of the ceria NPs measured by DLS.

Additionally, we conducted zeta potential measurements on the ceria NPs as a function of pH to verify the influence of aqueous conditions, as shown in Fig. S3a. The zeta potential of the ceria NPs decreased with increasing pH, yielding an intrinsic isoelectric point (IEP) ranging from 6 to 9, which falls within the typical IEP range of ceria [30]. The hydroxyl functional groups on the particle surfaces become ionized in aqueous media, exhibiting different forms of $-\text{OH}^{2+}$, $-\text{OH}$, and $-\text{O}^-$ with varying pH levels from low to high.

The high zeta potential value plays a pivotal role in maintaining high dispersion stability, subsequently impacting the CMP process. For instance, particle aggregation can lead to a reduction in particle-wafer contact, thereby degrading CMP performance. Moreover, these aggregated particle clusters can slide on the wafer surface, causing scratches. DLS analysis can directly provide the hydrodynamic radius of the particles, indicating whether they are aggregated or not, as shown in Fig. 5b. At pH 4, where the ceria NPs exhibit high zeta potential values, the particles are highly dispersible, showing sizes almost identical to those measured from the TEM and SEM images (see Fig. 1d). This suggests that the particles are dispersed individually in water, exhibiting narrow size distributions, particularly for the NC-ceria NPs. In sharp contrast, near the IEP, the particles are likely to lose dispersibility due to weak surface charge, aggregate with each other, and precipitate easily. The digital photos in Fig. S3b compare the aqueous dispersion of NC51 at pH 4 and 7 (near the IEP). When attempting to measure the hydrodynamic radius of NC51 using its aqueous dispersion near the IEP, it was found to be out of range (i.e., $> 6,000$ nm), indicating particle aggregation.

Fig. 6 shows a comparison of the oxide RRs of slurries containing three NC-ceria NPs (NC51, NC69, and NC108) and CF-ceria NPs (HC60) at a concentration of 0.3 wt%. All NC-ceria slurries exhibited significantly superior RRs compared with that of CF-ceria. Particularly, despite the similar sizes of the NC108 and HC60 NPs, the NC108 NPs exhibited a higher RR of 3546 Å/min compared to that of the cubic-fluorite NPs (2197 Å/min). This difference may be attributed to the significantly higher surface chemical activity of NC108 compared with that of CF-ceria. In other words, more Ce^{3+} and hydroxyl groups can be formed on the surface of NC-ceria.

The RR of NC-ceria slurry predominantly increased with decreasing particle size: 3546, 4392, and 5394 Å/min for NC108, NC69, and NC51, respectively. That is, the RR increased by 1848 Å/min as the size of the ceria NPs was approximately halved from 108.0 to 51.4 nm. This is consistent with the demonstrated tendency in Fig. 3 for particle size and $\text{Ce}^{3+}/\text{Ce}^{4+}$ surface chemistry to be inversely related. However, despite the surface properties of NC51 ($\text{Ce}^{3+}/\text{Ce}^{4+} = 81.7\%$, BET surface area = $136.2 \text{ m}^2/\text{g}$) being superior by approximately twice or more than those of NC108 ($\text{Ce}^{3+}/\text{Ce}^{4+} = 48.4\%$, BET surface area = $53.5 \text{ m}^2/\text{g}$),

the ~ 52 % increase in SiO_2 RR is a relatively minor improvement. This can be understood as a complex result influenced by N_p , S_p , and M_p , which vary with the particle size. For example, the NC51 NPs in the slurry are lighter than the NC108 NPs; therefore, the number of contacts to the SiO_2 substrate (N_p) may increase during the polishing process, while the S_p and M_p of each particle may decrease. In addition to these physical kinetics, the multifunctional action of chemical properties such as surface activity also played a role, resulting in a final SiO_2 -RR of 5394 Å/min, which is approximately 52 % higher than that of NC108. Moreover, besides the excellent RR of NC-ceria NPs, their round shape and narrow size distribution are likely to be more beneficial for reducing scratch defects in CMP processes.

After conducting the polishing tests, we evaluated the surface morphologies of the abrasive particles from the used slurries. As depicted in Fig. S4, NC51, NC69, NC108, and HC60 NPs maintained their original shapes after the tests. Particularly noteworthy is that the nanoclustered structures of the NC-ceria NPs, consisting of tiny granules, remained intact during the polishing process, indicating strong bonding between them. Additionally, SEM images in Fig. S5 compare the surface of the wafers before and after the test with different abrasives. The bare wafer before the test displays a smooth and clean surface (Fig. S5a). After the test with the slurries, all wafers showed the presence of abrasive particles uniformly distributed on their surfaces (Fig. S5b–S5e). This phenomenon is likely due to the strong affinity between the abrasives and the SiO_2 surface of the wafer via electrostatic attraction, as confirmed by zeta potential analysis. Furthermore, the formation of Ce–O–Si bonding during polishing also contributed to the presence of remaining abrasives on the wafer surfaces, which become more numerous with decreasing ceria NP size due to a higher concentration of Ce^{3+} . These factors are highly beneficial for achieving high SiO_2 RR, but they act as a drawback in the post-CMP cleaning process [33]. While the current study focuses on investigating the size effects of the NC-ceria NPs on surface activity and CMP performance, our ongoing study will introduce the cleaning process of these particles after polishing and examine the efficacy of various cleaning conditions.

4. Conclusions

Herein, we investigated the size dependence of NC-ceria NPs on chemical surface activity as well as RR, which represent CMP performance. We used uniform NPs with three diameters — 51.4 nm (NC51), 68.6 nm (NC69), and 108.0 nm (NC108) — that exhibit highly spherical shapes and narrow size distributions. These NC-ceria NPs, which were composed of aggregates of small crystalline and amorphous crystallites, exhibited substantially higher BET surface areas compared with those of conventional CF-ceria NPs, which increased with decreasing diameter. We also demonstrated that the NC-ceria NPs possessed a relatively low crystallinity of ~ 70.6 %, as opposed to that of the CF-ceria NPs (> 95 %). The surface activity (i.e., $\text{Ce}^{3+}/\text{Ce}^{4+}$) of the NC-ceria NPs also increased considerably with decreasing particle size, reaching 81.7 % for NC51. This chemical surface activity affects CMP performance because it is clearly related to the number of sites forming Si–O–Ce bonds during the polishing process. In addition to the chemical properties, several physical parameters related to the size of the abrasives can affect CMP performance. Overall, NC-ceria NPs outperformed conventional CF-ceria NPs on the aspect of SiO_2 -RR owing to their larger surface area and higher surface activity stemming from the presence of nanoclusters with low crystallinity.

CRediT authorship contribution statement

Na-Yeon Kim: Writing – original draft, Visualization, Methodology, Investigation, Conceptualization. **Uiseok Hwang:** Writing – review & editing, Validation, Investigation. **Jaeuk Sung:** Investigation. **In-Kyung Park:** Investigation. **Taesung Kim:** Funding acquisition. **Jonghwan Suhr:** Funding acquisition. **Jae-Do Nam:** Writing – review & editing,

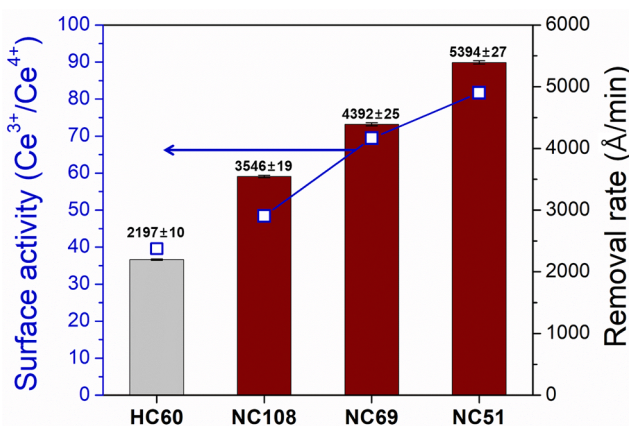


Fig. 6. SiO_2 -RRs of CMP slurries containing CF- and NC-ceria NPs with variations in RR.

Methodology, Funding acquisition, Conceptualization.

Declaration of competing interest

The authors declare that they have no known competing financial interests or personal relationships that could have appeared to influence the work reported in this paper.

Data availability

Data will be made available on request.

Acknowledgement

This work was supported by the Technology Innovation Program (20016548) funded by the Korean Government (Ministry of Trade, Industry & Energy (MOTIE)).

Appendix A. Supplementary data

Supplementary data to this article can be found online at <https://doi.org/10.1016/j.apsusc.2024.160123>.

References

- [1] R.R. Schaller, Moore's law: past, present and future, *IEEE Spectrum* 34 (6) (1997) 52–59, <https://doi.org/10.1109/6.591665>.
- [2] N. Collaert, A. Alian, H. Arimura, G. Boccardi, G. Eneman, J. Franco, T. Ivanov, D. Lin, R. Loo, C. Merckling, J. Mitard, M.A. Pourghaderi, R. Rooyackers, S. Sioncke, J.W. Sun, A. Vandooren, A. Veloso, A. Verhulst, N. Waldron, L. Witters, D. Zhou, K. Barla, A.V.Y. Thean, Ultimate nano-electronics: New materials and device concepts for scaling nano-electronics beyond the Si roadmap, *Microelectron. Eng.* 132 (2015) 218–225, <https://doi.org/10.1016/j.mee.2014.08.005>.
- [3] Y.-H. Son, J.-G. Park, B.-K. Choo, S.-B. Kang, Self-stopping slurry for planarizing extremely high surface film topography in nanoscale semiconductor devices, *J. Korean Phys. Soc.* 79 (1) (2021) 44–48, <https://doi.org/10.1007/s40042-021-00207-x>.
- [4] R. Srinivasan, P.V.R. Dandu, S.V. Babu, Shallow trench isolation chemical mechanical planarization: A review, *ECS J. Solid State Sci. Technol.* 4 (11) (2015) P5029–P5039, <https://doi.org/10.1149/2.0071511jss>.
- [5] H.J. Kim, Abrasive for chemical mechanical polishing, *Abrasive Technology: Characteristics and Applications* (2018). DOI: 10.5772/intechopen.75408.
- [6] N.-Y. Kim, G. Kim, H. Sun, U. Hwang, J. Kim, D. Kwak, I.-K. Park, T. Kim, J. Suhr, J.-D. Nam, A nanoclustered ceria abrasives with low crystallinity and high Ce³⁺/Ce⁴⁺ ratio for scratch reduction and high oxide removal rates in the chemical mechanical planarization, *J. Mater. Sci.* 57 (26) (2022) 12318–12328, <https://doi.org/10.1007/s10853-022-07338-x>.
- [7] Z. Li, D. Jia, W. Zhang, Y. Li, M. Wang, D. Zhang, Enhanced photocatalytic performance by regulating the Ce³⁺/Ce⁴⁺ ratio in cerium dioxide, *Front. Chem. Sci. Eng.* 18 (3) (2024) 31, <https://doi.org/10.1007/s11705-024-2394-4>.
- [8] J. Ma, N. Xu, Y. Luo, Y. Lin, Y. Pu, Enhancing the polishing efficiency of CeO₂ abrasives on the SiO₂ substrates by improving the Ce³⁺ concentration on their surface, *ACS Appl. Electron. Mater.* 5 (1) (2023) 526–536, <https://doi.org/10.1021/acsaeml.2c01553>.
- [9] J. Lee, E. Kim, C. Bae, H. Seok, J. Cho, K. Aydin, T. Kim, Improvement of oxide chemical mechanical polishing performance by increasing Ce³⁺/Ce⁴⁺ ratio in ceria slurry via hydrogen reduction, *Mater. Sci. Semicond. Process.* 159 (2023) 107349, <https://doi.org/10.1016/j.mssp.2023.107349>.
- [10] E. Kim, J. Lee, C. Bae, H. Seok, H.-U. Kim, T. Kim, Effects of trivalent lanthanide (La and Nd) doped ceria abrasives on chemical mechanical polishing, *Powder Technol.* 397 (2022) 117025, <https://doi.org/10.1016/j.powtec.2021.11.069>.
- [11] J.-D. Nam, N.-Y. Kim, I.-K. Park, U. Hwang, D. Kim, Spherical inorganic particles having surface bump and method for preparing same, Republic of Korea Patent 10-2261151 (2021).
- [12] J.-D. Nam, N.-Y. Kim, I.-K. Park, U. Hwang, D. Kim, Spherical inorganic particles having surface bump and method for preparing same, U.S. Patent App. 17/611,806 (2022).
- [13] S. Kurokawa, T. Toyama, T. Hayashi, E. Suda, J. Tokuda, Controllable CMP of oxide film by using colloidal ceria slurry, *ICPT 2017, International conference on planarization/ CMP technology*, Leuven, Belgium, 2017.
- [14] J. Tokuda, M. Yuasa, E. Suda, Zenus®, a new generation of colloidal ceria abrasives, *ECS Transactions* 60 (1) (2014) 653–657.
- [15] A. Monshi, M.R. Foroughi, M.R. Monshi, Modified Scherrer equation to estimate more accurately nano-crystallite size using XRD, *World J. Nano Sci. Eng.* 2 (3) (2012) 154–160, <https://doi.org/10.4236/wjnse.2012.23020>.
- [16] G.C.V. Iulianelli, G.d.S. David, T.N. dos Santos, P.J.O. Sebastião, M.I.B. Tavares, Influence of TiO₂ nanoparticle on the thermal, morphological and molecular characteristics of PHB matrix, *Polym. Test.* 65 (2018) 156–162, <https://doi.org/10.1016/j.polymertesting.2017.11.018>.
- [17] C. Zhang, J. Lin, Visible-light induced oxo-bridged Zr(IV)-O-Ce(III) redox centre in tetragonal ZrO₂-CeO₂ solid solution for degradation of organic pollutants, *Phys. Chem. Chem. Phys.* 13 (9) (2011) 3896–3905, <https://doi.org/10.1039/c0cp01782e>.
- [18] C.M. Sims, R.A. Maier, A.C. Johnston-Peck, J.M. Gorham, V.A. Hackley, B. C. Nelson, Approaches for the quantitative analysis of oxidation state in cerium oxide nanomaterials, *Nanotechnol.* 30 (8) (2019) 085703, <https://doi.org/10.1088/1361-6528/aae364>.
- [19] S. Deshpande, S. Patil, S.V. Kuchibhatla, S. Seal, Size dependency variation in lattice parameter and valency states in nanocrystalline cerium oxide, *Appl. Phys. Lett.* 87 (13) (2005), <https://doi.org/10.1063/1.2061873>.
- [20] J. Seo, A. Gowda, S.V. Babu, Almost complete removal of ceria particles down to 10 nm size from silicon dioxide surfaces, *ECS J. Solid State Sci. Technol.* 7 (5) (2018) P243–P252, <https://doi.org/10.1149/2.0131805jss>.
- [21] X. Hao, A. Yoko, C. Chen, K. Inoue, M. Saito, G. Seong, S. Takami, T. Adscharis, Y. Ikuhara, Atomic-scale valence state distribution inside ultrafine CeO₂ nanocubes and its size dependence, *Small* 14 (42) (2018) 1802915, <https://doi.org/10.1002/smll.201802915>.
- [22] S.D. Senanayake, D. Stacchiola, J. Evans, M. Estrella, L. Barrio, M. Pérez, J. Hrbek, J.A. Rodriguez, Probing the reaction intermediates for the water–gas shift over inverse CeO_x/Au(111) catalysts, *J. Catal.* 271 (2) (2010) 392–400, <https://doi.org/10.1016/j.jcat.2010.02.024>.
- [23] C. Zhang, Y. Yu, M.E. Grass, C. Dejoie, W. Ding, K. Gaskell, N. Jabeen, Y.P. Hong, A. Shavorskiy, H. Bluhm, W.X. Li, G.S. Jackson, Z. Hussain, Z. Liu, B.W. Eichhorn, Mechanistic studies of water electrolysis and hydrogen electro-oxidation on high temperature ceria-based solid oxide electrochemical cells, *J. Am. Chem. Soc.* 135 (31) (2013) 11572–11579, <https://doi.org/10.1021/ja402604u>.
- [24] L.M. Cook, Chemical processes in glass polishing, *J. Non-Cryst. Solids.* 120 (1990) 152–171, [https://doi.org/10.1016/0022-3093\(90\)90200-6](https://doi.org/10.1016/0022-3093(90)90200-6).
- [25] P.R.V. Dandu, B.C. Peethala, S.V. Babu, Role of different additives on silicon dioxide film removal rate during chemical mechanical polishing using ceria-based dispersions, *J. Electrochem. Soc.* 157 (9) (2010) H869–H874, <https://doi.org/10.1149/1.3457387>.
- [26] T. Andana, M. Piumenti, S. Bensaid, N. Russo, D. Fino, R. Pirone, CO and soot oxidation over Ce-Zr-Pr oxide catalysts, *Nanoscale Res. Lett.* 11 (1) (2016) 278, <https://doi.org/10.1186/s11671-016-1494-6>.
- [27] P. Wang, Aggregation of TiO₂ nanoparticles in aqueous media: effects of pH, ferric ion and humic acid, *Int. J. Environ. Sci. Nat. Res.* 1 (5) (2017), <https://doi.org/10.19080/ijesn.2017.01.555575>.
- [28] J. Seo, J. Moon, J.H. Kim, K. Lee, J. Hwang, H. Yoon, D.K. Yi, U. Paik, Role of the oxidation state of cerium on the ceria surfaces for silicate adsorption, *Appl. Surf. Sci.* 389 (2016) 311–315, <https://doi.org/10.1016/j.apsusc.2016.06.193>.
- [29] H.-G. Kang, T. Katoh, S.-J. Kim, U. Paik, H.-S. Park, J.-G. Park, Effects of grain size and abrasive size of polycrystalline nano-particle ceria slurry on shallow trench isolation chemical mechanical polishing, *Jpn. J. Appl. Phys.* 43 (3A) (2004) L365, <https://doi.org/10.1143/JJAP.43.L365>.
- [30] U. Hwang, J. Kim, N.-Y. Kim, K. Choi, J.-Y. Chung, T. Kim, J. Suhr, J.-D. Nam, Surface charge control of hierarchical ceria/silica hybrid shells for enhanced dispersion stability, *Appl. Surf. Sci.* 571 (2022) 151173, <https://doi.org/10.1016/j.apsusc.2021.151173>.
- [31] Y. Chen, J. Lu, Z. Cehen, Preparation, characterization and oxide CMP performance of composites polystyrene-core ceria-shell abrasives, *Microelectron. Eng.* 88 (2) (2011) 200–205, <https://doi.org/10.1016/j.mee.2010.10.019>.
- [32] T. Wang, Y. Chen, A. Chen, Y. Chen, Development of carbon sphere/ceria (CS/CeO₂) heterostructured particles and their applications to functional abrasives toward photochemical mechanical polishing, *Appl. Surf. Sci.* 593 (15) (2022) 153449, <https://doi.org/10.1016/j.apsusc.2022.153449>.
- [33] S. Sahir, N.P. Yerriboina, S.-Y. Han, T.-G. Kim, N. Mahadev, J.-G. Park, Mechanisms of colloidal ceria contamination and cleaning during oxide post CMP cleaning, *Microelectron. Eng.* 241 (15) (2021) 111544, <https://doi.org/10.1016/j.mee.2021.111544>.